Sound propagation in and low frequency noise absorption by helium-filled porous material

Y. S. Choy[a)]
Department of Mechanical Engineering, The Hong Kong Polytechnic University, Kowloon, Hong Kong

Lixi Huang and Chunqi Wang
Department of Mechanical Engineering, The University of Hong Kong, Pokfulam Road, Hong Kong

(Received 20 January 2009; revised 17 September 2009; accepted 20 September 2009)

Low-frequency noise is difficult to deal with by traditional porous material due to its inherent high acoustic impedance. This study seeks to extend the effective range of sound absorption to lower frequencies by filling a low density gas, such as helium, in the porous material. Compared with conventional air-filled absorption material, the helium-filled porous material has a much reduced characteristic impedance; hence, a good impedance matching with pure air becomes more feasible at low frequencies. The acoustic properties of a series of helium-filled porous materials are investigated with a specially designed test rig. The characteristic of the sound propagation in a helium-filled porous material is established and validated experimentally. Based on the measured acoustic properties, the sound absorption performance of a helium-filled absorber (HA) of finite thickness is studied numerically as well as experimentally. For a random incidence field, the HA is found to perform much better than the air-filled absorber at low frequencies. The main advantage of HA lies in the middle range of oblique incidence angles where wave refraction in the absorber enhances sound absorption. The advantage of HA as duct lining is demonstrated both numerically and experimentally. © *2009 Acoustical Society of America.* [DOI: 10.1121/1.3257182]

PACS number(s): 43.55.Ev, 43.20.Jr [KVH] Pages: 3008–3019

I. INTRODUCTION

The porous sound absorption material has been the backbone of the noise control industry. But there are still technical challenges for the porous materials to deal with the low frequency noise effectively. The main technical challenge is associated with its high magnitude of the characteristic impedance at low frequencies. As the sound wave propagates through the porous material, the porous fibers exert a drag force on the oscillating air particles. At the same time, the irregular changes of air flow direction by the fibers cause a virtual mass. The drag force and the virtual mass can be grouped together as an inertia term to form the complex density of the porous material (Zwikker and Kosten, 1949). The imaginary part of the complex density derives from the conversion of the friction force, which is proportional to the air particle velocity, to an inertia term associated with the acceleration. This imaginary part is inversely proportional to the frequency and thus becomes very large at low frequencies. Therefore, the characteristic impedance of the commonly used porous material is very large at low frequencies. Because of the high impedance mismatch between the porous material and the air, it is hard for the incident sound wave to enter the porous material and most of the incident wave will be reflected, hence the poor absorption performance at low frequencies. The large characteristic impedance might be reduced by increasing the porosity of the sound absorption material so that more sound waves can penetrate the absorber easily, but it requires a very thick absorption layer to dissipate sufficient amount of the low-frequency noise. Roughly speaking, a quarter wavelength is a desirable thickness for such absorber. For instance, the desirable thickness is about 8.5×10^{-1} m at the frequency of 100 Hz, which implies that the absorber required would be very bulky for the low-frequency noise control.

Aiming for a new sound absorbing device which works efficiently in the low frequency range, it is proposed to fill the pores of the porous sound absorption material with helium gas in this study, hence a helium-filled absorber (HA). The potential advantages of HA over the conventional air-filled absorber (AA) can be explained in two aspects. First, the low density of the helium gas helps to reduce the large characteristic impedance of the absorber, which is the major reason that causes the impedance mismatch at low frequency. Other light gases, such as hydrogen, can also be adopted for this purpose, but helium is chemically more stable than hydrogen. So, the inert gas of helium is preferred. The second potential benefit of HA arises from the higher speed of sound in helium than in air, the ratio being about 3. According to the rule of refraction, when sound wave is incident on HA at an oblique direction, which is by far the more usual situation encountered in practice than the perfectly normal incidence, the penetrated wave is bent toward the air-absorber interface. In contrast, the penetrated wave is bent toward the normal direction of the air-absorber interface for AA. Hence, the penetrated wave travels a longer path in HA before it is reflected back to the incident medium, which in turn implies more energy dissipation within a thin absorption layer.

[a)]Author to whom correspondence should be addressed. Electronic mail: mmyschoy@polyu.edu.hk

The investigation of the absorption performance of the helium-filled porous material requires the knowledge of its bulk acoustics properties such as the effective density and speed of sound, which does not seem to be available in existing literature. For air-filled porous material, empirical formulas have been well established based on the extensive measurements (Delany and Bazley, 1970; Mechel, 1976; Kirby and Cumming, 1999). These empirical formulas and the so-called semiempirical models (e.g., Allard and Champoux, 1992) are simple in form and convenient for use, but they are only intended for the air-filled porous material. On the other hand, efforts have also been made to characterize these properties analytically with various physical parameters of the porous media as well as the filling gas, for instance, the theoretical models developed by Johnson *et al.* (1987), Attenborough (1982, 1983, 1987), and Allard *et al.* (1986, 1989). The analytical models mentioned above apply to porous materials with any kind of filling gases, but the implementation of these models requires the knowledge of a number of parameters, some of which are difficult to measure in a common acoustic laboratory. In the current study, a dimensional analysis is carried out to determine the relationship between the bulk acoustic properties of the porous materials and various relevant physical parameters. Instead of seeking to establish a specific functionality between the acoustic properties and the relevant parameters, the dimensional analysis identifies dimensionless groups which can help predict the bulk acoustic properties of helium-filled porous materials based on the available data of air-filled porous medium. With proper assumptions made, the same functional relationship is deduced for absorber filled with air and that filled with helium as far as the porosity and geometrical shape of the fibers are the same. A series of experiments is carried out to determine the effective density and speed of sound of the helium-filled materials with different fiber diameters so that the acoustic properties of the helium-filled porous materials can be characterized. The experimental studies also validate the functional relations established in the dimensional analysis. Empirical regression curves which describe the dependency of the effective density and speed of sound on controlling parameters such as viscosity, size of the fiber, and density of the filling gas are deduced. With the acoustic properties obtained, the absorption behavior of a helium-filled finite-layer absorber is studied and compared with the commonly used AA for both random incidence and the grazing incidence in duct lining.

II. DIMENSIONAL ANALYSIS

Dimensional analysis is adopted to determine the relationships qualitatively between the bulk acoustic properties of the porous sound absorption materials (i.e., the complex characteristic impedance and propagation constant) and various other physical parameters. These physical variables can be classified into two main groups: geometrically related and fluid related. The geometrically related variables refer to those associated with the arrangement of the porous skeleton, e.g., the fiber diameter, the porosity derived from the ratio of the fiber diameter and the interfiber distance, and the wavelength. The relevant fluid-related variables include the fluid density, the speed of sound, which characterizes the fluid compressibility, and fluid viscosity. As the fluid passes through the pores, viscous damping occurs due to the friction between the fluid and the skeleton of the porous material. In order to investigate the variations in the characteristic impedance of the porous material filled with different gases, the two constitutional components of the characteristic impedance, i.e., the complex speed of sound c and the complex density ρ inside the porous material, are analyzed separately,

$$c = F(\mu, f, d, \rho_{\text{gas}}, c_{\text{gas}}, d_L) \quad \text{and} \quad \rho = G(\mu, f, d, \rho_{\text{gas}}, c_{\text{gas}}, d_L), \tag{1}$$

where μ is the dynamic viscosity, f is the frequency, d is the fiber diameter, ρ_{gas} is the fluid density, c_{gas} is the sound speed of the fluid in free field, and d_L is the mean distance between fibers. The effect of heat transfer can also be included in a manner similar to that for the viscous effect, but no extra control parameter arises when the Prandtl number of the fluid media is close to unity. Based on Buckingham theorem (Buckingham, 1914) in dimensional analysis, both the dependent variables (c and ρ) and the independent variables (μ, f, d, d_L, ρ_{gas}, and c_{gas}) are expressed in terms of the three fundamental physical quantities such as mass, length, and time. As a result, the normalized complex speed of sound c/c_{gas} and the normalized complex density ρ/ρ_{gas} depend on three dimensionless groups as follows:

$$\frac{c}{c_{\text{gas}}} = F\left(H, \frac{fd}{c_{\text{gas}}}, \frac{f\rho_{\text{gas}}d^2}{\mu}\right) \quad \text{and} \quad \frac{\rho}{\rho_{\text{gas}}} = G\left(H, \frac{fd}{c_{\text{gas}}}, \frac{f\rho_{\text{gas}}d^2}{\mu}\right). \tag{2}$$

The first dimensionless variable H in Eq. (2) is the porosity of the porous material, which is a crucial parameter for controlling the flow resistance. The second independent dimensionless variable is expressed as the fiber diameter normalized by the wavelength in the pure fluid, denoted by λ. The third independent dimensionless variable, $f\rho_{\text{gas}}d^2/\mu$, is proportional to frequency, the fluid density, and the square of the pore size but inversely proportional to the fluid viscosity. This term can be interpreted as the ratio of the fiber diameter to the boundary layer thickness δ with the power of 2, where $\delta = 5\sqrt{\mu/\rho\omega}$ (Lighthill, 1978).

The effects of the second and third dimensionless groups on the acoustical properties of porous material can be analyzed and compared as follows. Except for ultrasonic frequency ranges, the wavelength λ is normally much larger than the fiber diameter. Since the main geometric effect is represented by porosity and the main dynamic (force) effect derives from the fluid viscosity, the ratio d/λ may be interpreted as an indication of the effect of the fiber "individuality," which is not considered when the absorption material is treated as an equivalent fluid. On the other hand, the ratio of the fiber diameter to the acoustic boundary layer thickness d/δ signifies the main dynamic effect that the fibers have on the oscillating fluid particles, and it is typically much larger than d/λ. Therefore, the effect of the second independent variable fd/c_{gas} (i.e., d/λ) can be neglected, much like the way the weak influence of the Reynolds number has on lift

and drag coefficients that is excluded when the Reynolds number is very large (Lighthill, 1978). The number of independent variables is thus reduced from 3 to 2. Before the above assumption is adopted, the following numerical comparison between the three length scales is given for one specific configuration for reference. For a rectangular duct of height $h=0.1$ m, in room air condition, the boundary layer thickness δ and the wavelength λ are found to be $\delta=2.4\times10^{-4}$ m and $\lambda=3.43\times10^{-1}$ m at frequency $f=1000$ Hz. If the fiber diameter is $d=3\times10^{-5}$ m, then $d/\lambda=8.7\times10^{-5}$ and $d/\delta=0.13$. The corresponding ratios in helium are $d/\lambda=2.9\times10^{-5}$ and $d/\delta=0.046$, respectively. On neglecting the effect of d/λ, the normalized parameters are expressed as the new functions of porosity H and $f\rho_{\text{gas}}d^2/\mu$, denoted below by a new symbol E,

$$\frac{c}{c_{\text{gas}}}=F(H,E) \quad \text{and} \quad \frac{\rho}{\rho_{\text{gas}}}=G(H,E) \quad \text{where} \quad E=\frac{f\rho_{\text{gas}}d^2}{\mu}. \tag{3}$$

A series of experiments is carried out to establish the nature of these two functions with respect to E for a few given porosity H in Sec. III. The experimental evidence will also validate that the same functions of $F(H,E)$ and $G(H,E)$ do apply to both helium and air-filled absorption materials of the same geometrical shape. As already mentioned in the Introduction, specific functionalities have been established between the bulk acoustic properties and a series of physical parameters in previous theoretical models (Johnson *et al.* 1987; Attenborough, 1982, 1983, 1987; Allard *et al.*, 1986, 1989). According to theses models, for given geometrical configuration, the effective density normalized by that of the pure filling gas is dependent on the single variable $E_0=\rho_{\text{gas}}f/\mu$. For example, the normalized effective density in Johnson's model (Johnson *et al.*, 1987) can be expressed as

$$\frac{\rho}{\rho_{\text{gas}}}=\alpha_\infty\left(1+i\frac{H}{2\pi\alpha_\infty\kappa E_0}\sqrt{1-i\frac{8\pi\alpha_\infty^2\kappa^2}{H^2\Lambda^2}E_0}\right),$$

where the tortuosity α_∞, the Darcy constant κ, the porosity H, and the characteristic length Λ only depend on the geometrical configuration of the porous media. Thus, Johnson's model indicates that ρ/ρ_{gas} is solely determined by $E_0=\rho_{\text{gas}}f/\mu$ for given geometrical parameters. The effective speed of sound can be deduced from either Attenborough's (1982, 1983, 1987) or Allard *et al.*'s (1986, 1989) model. For given geometrical parameters, the theoretical models suggest that the ratio c/c_{gas} is a function of $E_0=\rho_{\text{gas}}f/\mu$, the specific heat ratio γ, and the Prandtl number B. For the helium gas and air considered in this study, it can be shown that the ratio c/c_{gas} is mainly determined by E_0 and the effect of γ and B can be neglected. In other words, for given geometrical parameters, the ratio c/c_{gas} can be approximately expressed as a function of E_0 in the theoretical models developed by Attenborough (1982, 1983, 1987) and Allard *et al.* (1986, 1989). Note that the fiber diameter d in the dimensionless parameter $E=f\rho_{\text{gas}}d^2/\mu$ in Eq. (3) is constant for given porous material. It can be seen that functional relations in Eq. (3) is consistent with the three above-mentioned theoretical models.

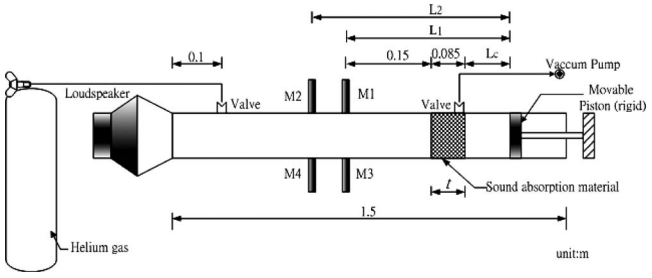

FIG. 1. Experimental set-up for the measurement of acoustical properties of porous materials filled with air or helium (dimensions: m).

III. EXPERIMENTAL STUDY AND REGRESSION ANALYSES

Three kinds of materials with different fiber diameters are tested with the experimental set-up shown in Fig. 1. The tube is specially designed for filling different kinds of gases under air-tight condition, namely, no leakage of gas. To ascertain this condition, the tube is calibrated by measuring and checking the speed of sound when helium gas is filled.

A. Calibration of the helium tube

The speed of sound of the helium gas in the test rig is measured with the test specimen (sound absorption material) absent in the experimental set-up. As shown in Fig. 1, when an incident sound wave hits the rigid piston, it will be reflected totally, and standing wave occurs in the tube. Below the first cut-on frequency, the sound pressures measured at M1 and M2 satisfy

$$p_1\cos(k_{\text{gas}}L_2)=p_2\cos(k_{\text{gas}}L_1), \tag{4}$$

where L_1 and L_2 are the distances between the surface of the movable piston and the microphones M1 and M2, respectively. To solve Eq. (4) for wavenumber k_{gas}, it is first expanded as

$$k_{\text{gas}}=k_0+\Delta k \quad \text{with} \quad k_0=\omega/c_{0,\text{gas}}, \tag{5}$$

where $c_{0,\text{gas}}$ is the nominal speed of sound in the filling gas (helium or air) indicated by the handbook (Zuckerwar, 2002), and Δk is the deviation of the measured wavenumber from the nominal value k_0 due to gaseous impurities and variation in environmental conditions. Assuming a small deviation Δk, the following approximation

$$e^{ik_{\text{gas}}L}\approx e^{ik_0L}(1+\Delta kL) \tag{6}$$

may be applied. By substituting Eq. (6) into Eq. (4), it gives

$$\Delta k=\frac{p_2\cos(k_0L_1)-p_1\cos(k_0L_2)}{p_2L_1\sin(k_0L_1)-p_1L_2\sin(k_0L_2)}. \tag{7}$$

Expanding Δk into the real and imaginary parts such that $\Delta k=\Delta k_r+i\Delta k_i$, the actual speed of sound in the gas is found as

$$c_{\text{gas}}=\omega/(k_0+\Delta k_r). \tag{8}$$

Figure 2 shows the measured (open circle) and the nominal (solid line) speed of sound of helium gas in room condition, together with the measured (triangle) and nominal (dashed line) speed of sound of air inside the same tube. The nominal

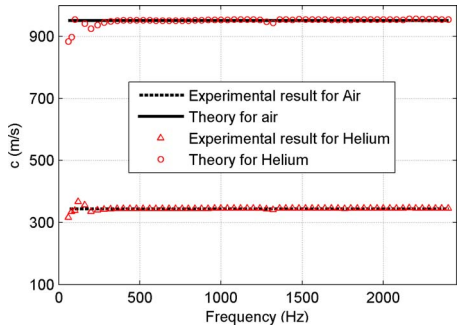

FIG. 2. (Color online) The speed of sound of helium- and air-filled inside the experimental testing tube.

speed of sound in air is 343 m/s for the particular temperature condition, while the experimental result is 340 m/s on average. For the helium gas, the nominal speed of sound is 970 m/s, while the measured value is about 975 m/s. On the whole, the measured speed of sound is in good agreement with the nominal value, especially in the relatively high frequency range (say, above 250 Hz). The measured speed of sound deviates from the nominal value gradually as the frequency approaches the very low frequency range (below 250 Hz). The largest deviation is observed at the lowest frequency, with the largest relative error of about 7% at the lowest frequency tested (120 Hz). The increased deviation may be attributed to the usual data uncertainty at extremely low frequencies due to the effect of the rig vibration. Nevertheless, it is considered to be acceptable for measuring the acoustical parameters of gas-filled porous material by using this test rig.

B. Methodology

The characteristic impedance and propagation constant are the prime parameters to be determined in order to find out the effective density and the speed of sound inside the porous material. Decomposition of these two parameters from the measurement of sound wave requires two distinct impedance conditions. Smith and Parrot (1983) achieved the distinct impedances by using two different thicknesses of material backed by a rigid cavity and this is called the two-thickness method. This method is not convenient for the current study because of the need to change the specimen inside the tube. On the other hand, Utsuno *et al.* (1989) introduced the improved two-cavity method in which two distinct impedances can be offered by changing the acoustic impedance behind the material. This can be achieved by adjusting the depth of the space behind the material. The thickness of the material remains the same in this method, so it is adopted for the current investigation of the acoustic properties of helium-filled material.

The experimental set-up for testing different kinds of absorption materials filled with different gases is shown in Fig. 1. The test tube, which has an internal diameter of 6×10^{-2} m and a total length of 1.5 m, is terminated by a movable rigid piston. The other end of the tube is connected to a loudspeaker. In order to avoid leakage of the filling gas, the surface of the cone of the loudspeaker is covered by a thin plastic membrane. The first cut-on frequency of the test tube is about 2850 Hz when air is filled and 7900 Hz when helium is filled. Since the density of helium gas is far less than that of air, the measurement frequency range was extended above the first cut-on frequency but still below the second cut-on frequency, so that the enough overlapping range of $E=f\rho_{\text{gas}}d^2/\mu$ between helium and air can be observed. For instance, the range of E for helium is extended from $E=2.8$ (below the first cut-on) to $E=5$ in Figs. 4(1a)–4(1d). It is known that, below the second cut-on frequency, both plane-wave mode and the first acoustic mode may occur in the test tube. As shown in Fig. 1, four microphones are used to resolve the plane-wave components from the standing wave pattern in the tube. The four microphones were calibrated before the measurement according to ISO 10534-2 (1998). By averaging the pressures at M1 (M2) and M3 (M4), the first acoustic mode is eliminated and only the plane-wave mode is kept, see Eqs. (9) and (10). Two microphone spacings were used for different frequency ranges during the measurement. In the low frequency range ($f\leq1900$ Hz for air-filled tube and $f\leq5300$ Hz for helium-filled tube), the separation distance between the two pairs of microphones was 8×10^{-2} m. In the high frequency range (1900 Hz$<f\leq5000$ Hz for air-filled tube and 5300 Hz $<f\leq11000$ Hz for helium-filled tube), a smaller separation distance of 3×10^{-2} m was used. There are two valves placed at 6×10^{-2} and 7.8×10^{-1} m away from the left end of the tube for air suction and gas injection, respectively. The movable piston is first used to place the testing samples in the appropriate position. Once the position of the specimen is fixed, the rigid piston is moved backward to create the space of depth L_c, which is measured by the scale attached onto the tube. The distance between the front surface of the testing material and the microphone M1 is adjusted to be 1.5×10^{-1} m. An air pump shown in Fig. 1 is used to discharge the air from the tube via a valve at one end while the helium gas is injected simultaneously into the tube from the other end. The pressure in the tube is monitored via a pressure gauge during the entire injecting and discharging procedure that lasts for at least 5 min. This is to ensure that the tube is completely filled with helium gas with minimum trace of air remaining in the tube. After the injection of helium gas, a signal with pre-set frequency range is generated from the loudspeaker, and the transfer function between the two microphones, M1 and M2, can be acquired. The incident noise is simulated by this loudspeaker. Two pairs of 0.5 in. microphones are used together with a conditioning amplifier to acquire the reasonably high signal-to-noise ratio. By using four microphones, the frequency range can be extended to 5000 Hz when it is air-filled and 11 000 Hz when it is helium-filled.

Formulations for the calculations of the characteristic impedance and propagation constant are briefly presented below. With the sound pressures measured by microphones M1–M4, the plane-wave components of the incident wave I and the reflected wave R can be found as follows:

$$I=\frac{(p_1+p_3)e^{-ik_{\text{gas}}L_2}-(p_2+p_4)e^{-ik_{\text{gas}}L_1}}{-i4\,\sin[k_{\text{gas}}(L_2-L_1)]}, \tag{9}$$

$$R = \frac{(p_2 + p_4)e^{ik_{\text{gas}}L_1} - (p_1 + p_3)e^{ik_{\text{gas}}L_2}}{-i4\,\sin[k_{\text{gas}}(L_2 - L_1)]}. \tag{10}$$

As a result, the acoustic impedance Z at the surface of the porous material is

$$Z = \frac{I + R}{I - R}\rho_{\text{gas}}c_{\text{gas}}, \tag{11}$$

and it can be expressed in terms of the characteristic impedance Z_c, the propagation constant k of the porous material, as well as the thickness of the porous material t under test (Utsuno *et al.*, 1989),

$$Z = Z_c \cdot \frac{-i\rho_{\text{gas}}c_{\text{gas}}\,\cot(k_{\text{gas}}L_c)\cosh(kt) + Z_c\,\sinh(kt)}{-i\rho_{\text{gas}}c_{\text{gas}}\,\cot(k_{\text{gas}}L_c)\sinh(kt) + Z_c\,\cosh(kt)}, \tag{12}$$

where ρ_{gas}, c_{gas}, and k_{gas} are, respectively, the density, the speed of sound, and the wavenumber of the pure gas in free space. In order to get the second surface impedance, the cavity depth is changed from L_c to L_c' by adjusting the movable piston. The resulting surface impedance of the testing sample is denoted as Z'. During the process of cavity depth change, the thickness of the testing sample remains unchanged. With the two surface acoustic impedances Z and Z' measured, the characteristic impedance Z_c and the propagation constant k inside the porous material can be found as

$$Z_c = \pm\sqrt{\frac{ZZ'(-i\rho_{\text{gas}}c_{\text{gas}})[\cot(k_{\text{gas}}L_c) - \cot(k_{\text{gas}}L_c')] + \rho_{\text{gas}}^2c_{\text{gas}}^2\,\cot(k_{\text{gas}}L_c)\cot(k_{\text{gas}}L_c')(Z - Z')}{-i\rho_{\text{gas}}c_{\text{gas}}[\cot(k_{\text{gas}}L_c) - \cot(k_{\text{gas}}L_c')] - (Z - Z')}} \tag{13}$$

and

$$k = \frac{1}{i2t}\ln\left[\frac{(Z + Z_c)}{Z - Z_c}\cdot\frac{-i\rho_{\text{gas}}c_{\text{gas}}\,\cot(k_{\text{gas}}L_c) + Z_c}{-i\rho_{\text{gas}}c_{\text{gas}}\,\cot(k_{\text{gas}}L_c) - Z_c}\right]. \tag{14}$$

The complex speed of sound and density of the porous material are then calculated by $c = \omega/k$ and $\rho = Z_c/c$, respectively. Note that the cavity depth L_c and L_c' should be carefully chosen so that two distinct sets of data can be measured. In this study, the cavity depths are $L_c = 4 \times 10^{-2}$ m and $L_c' = 1.1 \times 10^{-1}$ m for AA. For HA, since the wavelength of the helium gas is longer, a set of larger cavity depth, $L_c = 5 \times 10^{-2}$ m and $L_c' = 2.45 \times 10^{-1}$ m, is chosen.

C. Results

Three different porous materials are tested. They are as follows: (1) polyethylene foam with diameters of 2×10^{-4}, 3×10^{-4}, and 5×10^{-4} m; (2) polyester fiber material with a fiber diameter of 3×10^{-5} m; and (3) metal bead with a pore size of 4×10^{-3} m. All the testing samples are prepared as a circular cylinder of 6×10^{-2} m in diameter and 8.5×10^{-2} m in length. Following the apparent density method (Palacio, *et al.*, 1999), the porosity of the polyethylene foam, polyester fibers, and metal bead are found to be $H = 0.97$, 0.97, and 0.2, respectively. In the following presentation, the measured complex speed of sound c and effective density ρ of the porous materials are normalized as c/c_{gas} and ρ/ρ_{gas}, where c_{gas} and ρ_{gas} are the speed of sound and density of the corresponding filling gas in free space, respectively.

The results for the air-filled polyethylene foam are presented in Fig. 3. Figures 3(a) and 3(b) show the real and imaginary components of the normalized speed of sound as a function of $E = f\rho_{\text{gas}}d^2/\mu$. The physical meaning of the dimensionless parameter E has been explained in Sec. II. Figures 3(c) and 3(d) show the real and imaginary components of the normalized effective density as a function of E. The open circles, triangles, and stars shown on the graphs represent the measured results with fiber diameters of 2×10^{-4}, 3×10^{-4}, and 5×10^{-4} m, respectively. It can be observed that the results for different diameters show similar dependency on E. Although deviations may be observed at certain points, for instance, the imaginary part of c/c_{gas} and the imaginary part of ρ/ρ_{gas} when E is between 0.8 and 1.2, the three sets of data overlap with each other on the whole. This overlapping trend appears to confirm that, for given porosity H, the normalized complex speed of sound c and effective density ρ of the porous materials are decided by the dimen-

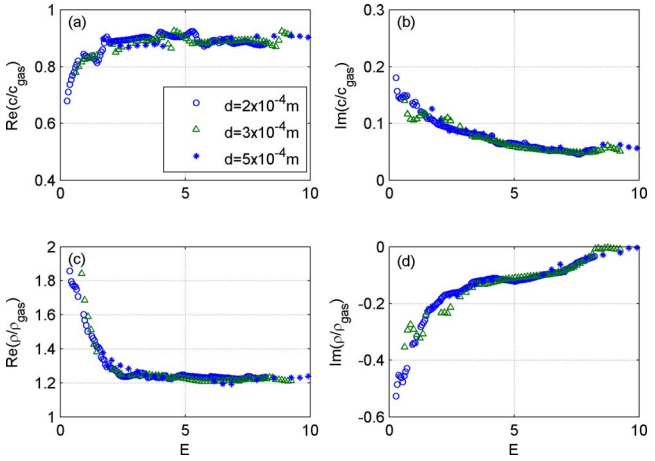

FIG. 3. (Color online) Characteristic of the polyethylene foam with different diameters and filled with air: (a) is the real part and (b) is the imaginary part of sound speed of the fluid in the porous material relative to that of air, respectively. (c) is the real part and (d) is imaginary part of effective density of porous material relative to that of air, respectively.

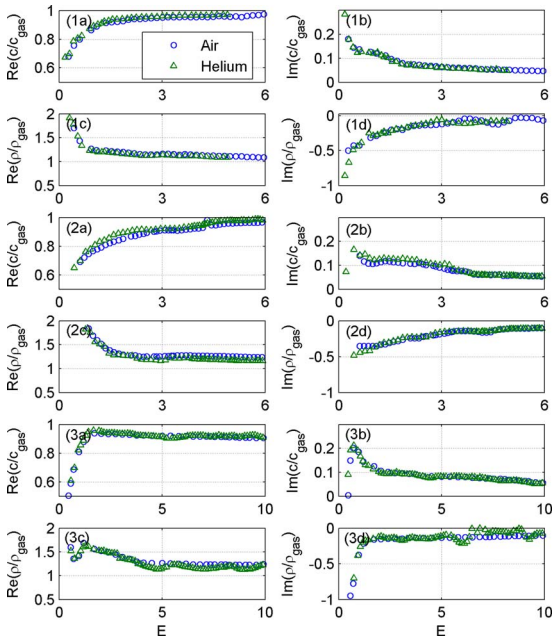

FIG. 4. (Color online) Characteristic of the polyethylene foam filled with helium (triangles) and air (circles). (1)–(3) represent the sponges with fiber diameters of 2×10^{-4}, 3×10^{-4}, and 5×10^{-4} m, respectively. For each set of subfigures, (a) is the real part and (b) is the imaginary part of sound speed of the fluid in the porous material relative to that of pure gas, respectively. (c) is the real part and (d) is the imaginary part of effective density of porous material relative to that of pure gas, respectively.

sionless parameter $E=f\rho_{\text{gas}}d^2/\mu$. This property can be employed to predict the acoustic properties of the air-filled porous material of other fiber diameters with the same porosity.

Figure 4 compares the measured acoustic properties for the helium-filled (triangles) and the air-filled (open circles) polyethylene foam as a function of $E=f\rho_{\text{gas}}d^2/\mu$. Three sets of subfigures, (1)–(3), are plotted for three different fiber diameters, 2×10^{-4}, 3×10^{-4}, and 5×10^{-4} m, respectively. In general, the normalized acoustic properties of the air-filled polyethylene foam coincide with those of the helium-filled polyethylene foam with little deviations. In the case of fiber diameter $d=2\times10^{-4}$ m, the maximum deviation of 0.06 is observed for the imaginary part of the normalized effective density, as shown in Fig. 4(1d). In the cases of fiber diameters $d=3\times10^{-4}$ and 5×10^{-4} m, the maximum deviation is found to be 0.05 in the low frequency range, as shown in Figs. 4(2d) and 4(3d). The deviation of 0.05 in the imaginary part of the effective density will cause a deviation of the normal absorption coefficient as large as 0.06, which can be neglected in many engineering applications. In other words, although the filling gases differ, the normalized acoustic properties of the porous materials show almost the same dependency on the dimensionless parameter, $E=f\rho_{\text{gas}}d^2/\mu$. Additionally, the smooth variation in the experimental results suggests that generalized regression curves can be made to characterize the normalized parameters of c/c_{gas} and ρ/ρ_{gas} for porous materials filled with different gases.

Glass fibers and polyester fibers are very commonly used in industry such as duct lining and acoustical treatment in room. Polyester fibers with fiber diameter $d=3\times10^{-5}$ m are tested here. Figure 5 shows the measured normalized

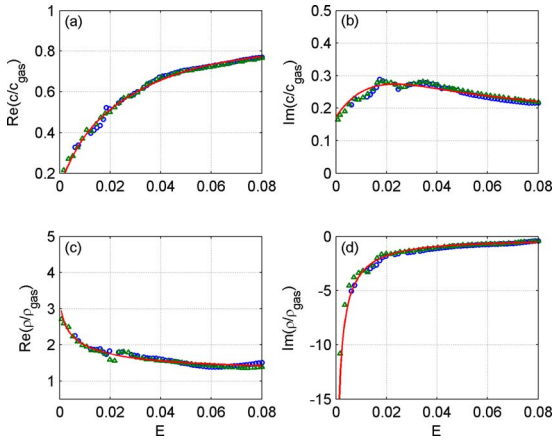

FIG. 5. (Color online) Characteristic of the polyester fiber with a fiber diameter of 3×10^{-5} m and filled with air (circles) and helium (triangles): (a) is the real part and (b) is the imaginary part of sound speed. (c) is the real part and (d) is the imaginary part of effective density, respectively. The solid lines show the regression curves based on the measured data of the air-filled polyester fiber.

acoustical parameters of air-filled (circles) and helium-filled (triangles) polyester fibers. Again, good agreement can be observed between the air-filled and helium-filled polyester fibers except at $E=0.02$ in Fig. 5(c), where a deviation of about 0.25 is observed for the real part of the normalized effective density. The same measurements are repeated for the air-filled and helium-filled metal beads with the diameter of 4×10^{-3} m, and similar observations can be made, as shown in Fig. 6.

Regression curves are deduced based on the measured data for air-filled polyester fiber in the forms of

$$\frac{c}{c_{\text{gas}}}=\sum_{m=0}^{4}a_mE^m+i\sum_{n=0}^{6}b_nE^n, \tag{15}$$

$$\frac{\rho}{\rho_{\text{gas}}}=\sum_{m=0}^{2}r_m(\log E)^m+i\sum_{n=0}^{4}s_n(\log E), \tag{16}$$

where a_m, b_n, s_n, and r_m are the regression parameters. The orders of the polynomial curves and the unknown regression

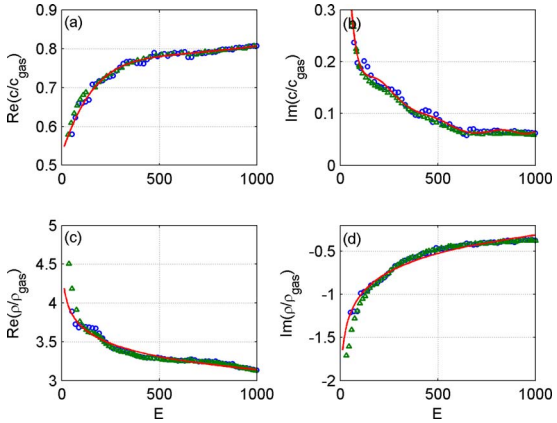

FIG. 6. (Color online) Characteristic of metal beads with diameter of 4×10^{-3} m and filled with air (circles) and helium (triangles): (a) is the real part and (b) is imaginary part of sound speed, (c) is the real part and (d) is the imaginary part of effective density, respectively. The solid lines show the regression curves based on the measured data of the air-filled metal beads.

TABLE I. The regression parameters for the empirical formulas for polyester fiber.

	$E \geq 0.12$	$E < 0.12$
a_0	0.792	0.147
a_1	0.511	27.89
a_2	−0.613	−553.62
a_3	0.284	5 081.88
a_4	−0.0467	−16 739.9
b_0	0.254	0.173
b_1	−0.742	11.65
b_2	1.32	−479.74
b_3	−1.311	8 926.6
b_4	0.717	−87 247
b_5	−0.202	430 398.8
b_6	0.023	−843 642.1
r_0	1.27	1.27
r_1	0.0154	0.0154
r_2	0.0291	0.0291
s_0	−0.06	−0.06
s_1	0.173	0.173
s_2	0.016	0.016
s_3	−0.017	−0.017
s_4	−0.01	−0.01

parameters are determined by minimizing the mean deviations between the measured results and the polynomial curves. The standard least-squares procedure is followed in the minimization of the mean deviations. Table I lists the regression parameters for the air-filled polyester fibers. The corresponding regression curves are plotted in Fig. 5. Although the regression curves are deduced using the measured results of the air-filled polyester fiber, they also match the measured results of the helium-filled materials.

As a summary, the complex speed of sound and the effective density of a variety of helium-filled porous materials are measured with an especially designed test rig. Since the helium gas changes the virtual mass and the flow resistance of the porous material greatly, the measured acoustic properties differ from those of the commonly used air-filled porous materials. However, it is found that the normalized parameters of c/c_{gas} and ρ/ρ_{gas} follow the same functional relationships of $c/c_{\text{gas}}=F(H,E)$ and $\rho/\rho_{\text{gas}}=G(H,E)$, where H is the porosity and $E=f\rho_{\text{gas}}d^2/\mu$. That is to say, following the normalization scheme described in Eq. (3), the acoustic properties of the helium-filled porous materials can be predicted from the existing data of the air-filled porous materials. This observation facilitates the analytical studies on the acoustic behaviors of porous materials saturated by gases other than air.

IV. ABSORPTION OF A HELIUM-FILLED FINITE-LAYER ABSORBER

To demonstrate the potential advantages of the helium gas filling in the porous absorption material, the performance of a HA of finite thickness is studied for both free field and confined space (duct). The polyester fiber is selected as the sound absorption material. With the empirical formulas established in Eqs. (15) and (16), the acoustical properties of the polyester fiber with different fiber diameters can be predicted.

A. Absorption in free field

In free field, the noise sources can be plane waves at normal, oblique, or diffuse incidence. For a finite absorption layer of thickness t in front of a rigid wall, the absorption coefficient at oblique incidence θ_0 is (Attenborough and Vér, 2006)

$$\alpha(\theta_0)=\frac{4\,\text{Re}(Z)\cdot Z_0\cos\theta_0}{[\text{Re}(Z\cos\theta_0)+Z_0]^2+\text{Im}(Z\cos\theta_0)^2}$$

with

$$Z=\frac{(Z_c/\rho_0 c_0)}{\cos\theta}\coth(ikt\cos\theta), \tag{17}$$

where the incidence angle θ_0 is measured from the direction normal to the absorber surface, θ is the complex refraction angle in the absorber layer, and $Z_0=1$ is the specific acoustic impedance of air. According to the rule of refraction (Snell's law), the complex refraction angle satisfies the relationship

$$\cos^2\theta=1-\frac{k_0^2}{k^2}\sin^2\theta_0, \tag{18}$$

where $k_0=\omega/c_0$ is the free field wavenumber in air. In most situations, the sound will be incident on an absorptive material from a multitude of incident angles at once. Therefore, to account for a wide range of incidence angles, the statistic absorption coefficient α_{ran} is usually determined by summing the absorption coefficients at all angles of incidence, as defined below:

$$\alpha_{\text{ran}}=\int_0^{\pi/2}\alpha(\theta_0)\sin(2\theta_0)d\theta_0. \tag{19}$$

The absorption performance of the HA is calculated and compared with that of the AA, as shown in Fig. 7. Both absorbers have a thickness of $t=5\times10^{-2}$ m, while the porosity of the polyester fiber is $H=0.97$. Figures 7(a) and 7(b) plot the contours of the absorption coefficient under random incidence, α_{ran}, as a function of the fiber diameter d and the normalized frequency

$$f_d=ft/c_0, \tag{20}$$

where t is the thickness of the finite absorption layer, and c_0 is the free field speed of sound in air. Figure 7(a) shows that AA can achieve at least $\alpha_{\text{ran}}=0.5$ for normalized frequency $f_d>0.04$. For HA shown in Fig. 7(b), $\alpha_{\text{ran}}\geq0.5$ can be achieved for $f_d>0.014$. For higher absorption coefficient, e.g., $\alpha_{\text{ran}}=0.7$, the lower frequency limits of AA and HA are $f_d=0.062$ and 0.034, respectively. The above comparison suggests that HA has a great potential to enhance the sound absorption performance in the low frequency range. Meanwhile, the comparison between the two contour plots also shows that the most effective fiber diameters of the two absorbers differ from each other. Aiming to maximize the absorption capability of the finite-layer absorber, an optimiza-

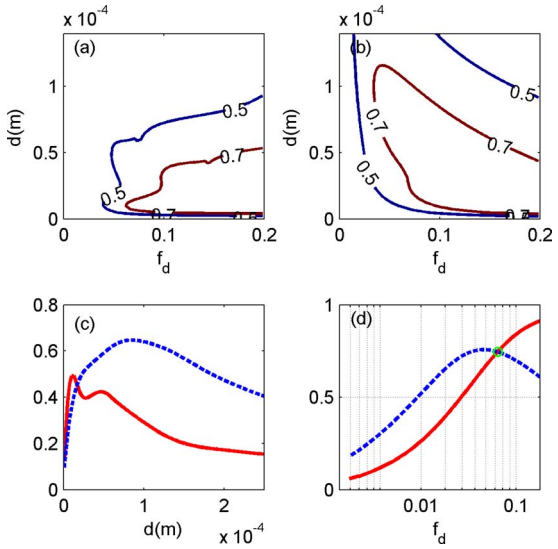

FIG. 7. (Color online) Performance optimization of the finite-layer absorbers (thickness $t=5\times10^{-2}$ m; porosity $H=0.97$). The top row shows the contour plots of the statistic absorption coefficient α_{ran} as a function of normalized frequency f_d and fiber diameter d for (a) the air-filled absorber and (b) the helium-filled absorber, respectively. (c) The variation in the overall (frequency integrated) absorption coefficient $\bar{\alpha}_{\text{ran}}$ as a function of the fiber diameter d (solid: air-filled; dashed: helium-filled). The two open circles mark the optimal diameters for the two absorbers. (d) Spectral comparison of the optimal absorption curves between the air-filled (solid) and the helium-filled (dashed) absorbers.

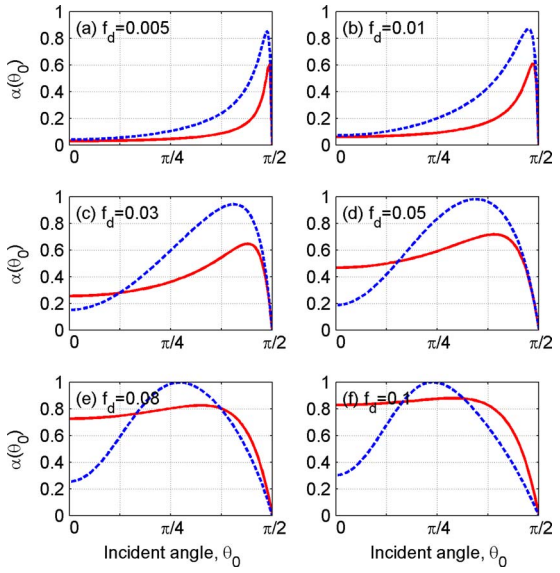

FIG. 8. (Color online) Absorption coefficients of the air-filled (solid lines) and helium-filled (dashed line) absorbers as a function of the angle of incidence θ_0. The porosity of the polyester fiber is $H=0.97$, the fiber diameter is $d=1\times10^{-5}$ m for the air-filled absorber, and $d=9\times10^{-5}$ m for the helium-filled absorber. The thickness for both absorbers is $t=5\times10^{-2}$ m.

tion procedure is necessary to find the most effective fiber diameters.

For given porosity $H=0.97$ and thickness $t=5\times10^{-2}$ m, the absorber performance is optimized by searching for the optimal fiber diameter d_{opt} so that the overall absorption coefficient is the highest within the frequency range of interest, $f_d=[f_1,f_2]$. Here, the overall absorption coefficient $\bar{\alpha}_{\text{ran}}$ is simply defined as

$$\bar{\alpha}_{\text{ran}}=\frac{\int_{f_1}^{f_2}\alpha_{\text{ran}}df_d}{f_2-f_1}. \tag{21}$$

Because special emphasis is put on the low frequency noise, the normalized frequency range of [0.00625,0.1] is investigated. The corresponding dimensional frequency range can be calculated as [42.5 Hz, 680 Hz], which falls into the low-to-medium frequency range in the RC II curves (Blazier, 1997). Figure 7(c) shows the variation in the overall absorption coefficient $\bar{\alpha}_{\text{ran}}$ in the specified frequency range as a function of fiber diameter d. The optimal fiber diameters for HA (dashed line) and AA (solid line) are marked by open circles. Figure 7(d) shows the statistic absorption coefficients predicted with the optimal fiber diameters. At very low frequencies (e.g., $f_d<0.04$), HA (dashed line) outperforms the AA (solid line) significantly. The overall noise absorption level of HA almost doubles that of the AA in this frequency region. The advantage of HA extends to the frequency range around $f_d=0.08$, beyond which the performance of HA becomes worse than that of AA. The reasons for the performance degradation of HA at high frequency are discussed in Sec. IV B.

Figure 8 compares the absorption coefficient $\alpha(\theta_0)$ of HA (dashed lines) and AA (solid lines) as a function of the angle of incidence. Figures 8(a)–8(f) depict the variation in the absorption coefficients at different frequencies. Two observations can be made here. First, at normal incidence angle ($\theta_0=0$), HA shows no advantages over AA. As shown in Figs. 8(a) and 8(b), both absorbers have little absorption at very low frequencies if the incident sound is perpendicular to the air-absorber interface. As the frequency increases, AA performs much better than HA, as illustrated in Figs. 8(c)–8(f). Second, the advantage of HA lies in its strong absorption capability at oblique incidence, especially in the middle range of the angle of incidence. As shown in Figs. 8(d)–8(f), almost total absorption occurs at $\theta_0=\pi/3$ ($f_d=0.05$) and at $\theta_0=\pi/4$ ($f_d=0.08,0.1$). As shown by the weighting function $\sin(2\theta_0)$ in Eq. (19), the absorption at angles around $\theta_0=\pi/4$ dominates the total noise absorption for random incidence. Therefore, in comparison with AA, HA demonstrates much better performance at low to middle frequencies. However, as the frequency increases further, this advantage of HA is offset by its relatively low absorption efficiency at small angles of incidence, as shown in Fig. 8(f).

B. Impedance analysis

The distinct absorption behavior of HA is analyzed by its unique impedance matching condition. As illustrated in Eq. (17), the surface impedance of the finite-layer absorber can be decomposed into two parts. The first part is the specific characteristic impedance of the sound absorbing material, Z_c/ρ_0c_0, where ρ_0c_0 is the characteristic impedance of air in free field. The second part is $\coth(ikt\cos\theta)/\cos\theta$, which characterizes the multiple reflected sound waves in the thin layer. At normal incidence, this part reduces to $\coth(ikt)$ as $\cos\theta=1$. In the following, the above two parts are simply called the characteristic impedance and the cavity impedance

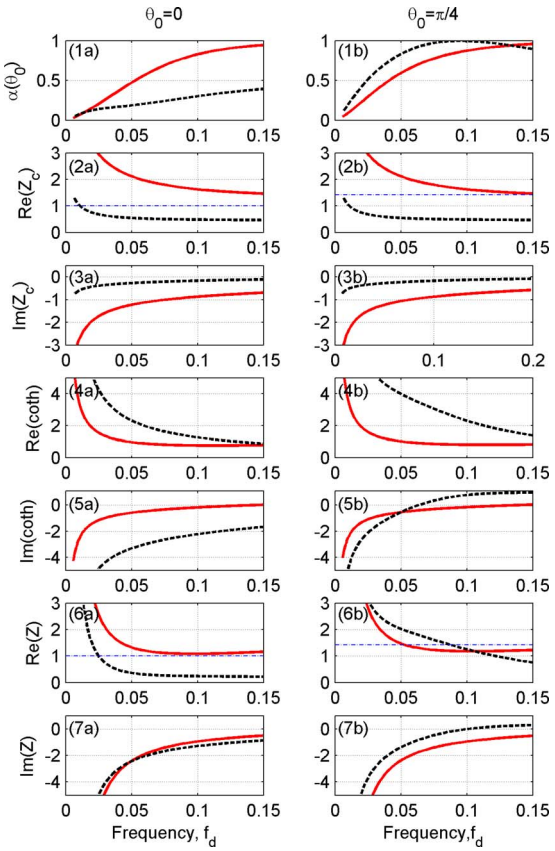

FIG. 9. (Color online) Impedance analysis of the air-filled (solid lines) and helium-filled (dashed lines) absorbers with the values of perfect match shown in dash-dot lines in some subfigures. The left column is for the normal incidence of $\theta_0=0$. The right column is for the oblique incidence with $\theta_0=\pi/4$. In (4a) and 5(a), "coth" means the cavity impedance $\coth(ikt\cos\theta)/\cos\theta$.

for convenience. Figure 9 shows the absorption coefficients and the corresponding acoustic impedances of the two absorbers at $\theta_0=0$ and $\pi/4$ (dashed lines: helium-filled; solid lines: air-filled). The physical properties of the sound absorption materials are the same as in Fig. 8.

The left column in Fig. 9 shows the results at normal incidence, $\theta_0=0$. At normal incidence, Figs. 9(2a) and 9(3a) just present the characteristic impedances of the helium-filled and air-filled polyester fibers normalized by that of air by setting $Z_0=1$. The characteristic impedance of the air-filled polyester fiber is too high, especially in the very low frequency range. The impedance mismatch between the air-filled polyester fiber and the incident wave reduces the chance of incident sound waves entering the absorber and being dissipated. On the contrary, the characteristic impedance of the helium-filled polyester fiber decreases from high to just under the value of unity as the frequency increases. Hence, an approximate impedance matching between the helium-filled polyester fiber and the incident field $(Z_0=1)$ can be observed in the frequency range $f_d \in [0.01, 0.03]$. However, in the case of normal incidence, HA does not perform better than AA, as indicated in Fig. 9(1a). The performance degradation of HA can be ascribed to its higher speed of sound and correspondingly longer acoustic wavelength. The longer acoustic wavelength makes the helium-filled absorber layer acoustically thinner than that of the air-filled

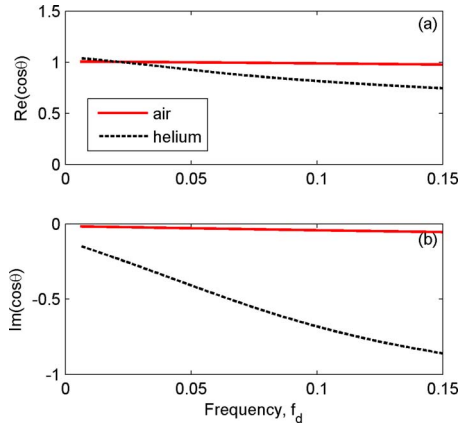

FIG. 10. (Color online) The cosine function of the complex refraction angle in the air-filled (solid lines) and the helium-filled (dashed lines) polyester fibers. (a) Real component and (b) imaginary component.

layer. Mathematically, it turns out to be a larger magnitude of the cavity impedance, $\coth(ikt)$, as shown in Figs. 9(4a) and 9(5a). Therefore, the total surface impedance of the helium-filled absorber, $Z_c \coth(ikt)/\rho_0 c_0$, still mismatches the impedance of the incident sound field $(Z_0=1)$ at low frequencies, as shown in Figs. 9(6a) and 9(7a). In other words, although the reduced characteristic impedance allows the incident noise to penetrate easily the helium-filled absorber, the thickness t is so thin compared with the acoustic wavelength that the incident noise has little chance of being dissipated before it is reflected by the rigid wall.

The right column in Fig. 9 shows the results when the angle of incidence is $\theta_0=\pi/4$. It can be seen that both absorbers have a better absorption performance than that at the normal incidence, but HA (dashed line) obviously outperforms AA (solid line) in this case. In order to find out the reasons for such performance difference, the effect of the oblique incidence angle on the acoustical behavior of AA is first investigated. Since the sound speed of the air-filled porous material is much slower than that in free space, the penetrated sound wave is bent toward the normal direction in the absorption layer. As shown in Fig. 10, for AA, the $\cos\theta$ is approximately equal to 1, which means that the penetrated sound wave is almost perpendicular to the air-absorber interface just as in the case of normal incidence. Hence, the acoustic impedance of AA is almost the same as that at normal incidence, see Eq. (17). The slight performance improvement of AA mainly derives from the changed impedance matching conditions relative to the situation of normal incidence. At oblique incidence, the absorption coefficient $\alpha(\theta_0)$ for the finite-layer absorber depends on how well the surface impedance Z matches the field impedance $Z_0/\cos\theta_0$ instead of Z_0. Note that the lack of impedance match at low frequencies is due to the overmatched surface impedance Z in many cases. Since the impedance mismatch is reduced by the increased field impedance $Z_0/\cos\theta_0=\sqrt{2}$ instead of $Z_0=1$, the absorption performance of AA is slightly improved in the low frequency range.

The effect of the oblique incidence angle on HA is more complicated but it can be shown to be beneficial. For HA, the characteristic impedances shown in Figs. 9(2b) and 9(3b)

remain the same as those in Figs. 9(2a) and 9(3a) (dashed line). However, as the incident field impedance becomes $Z_0/\cos\theta_0=\sqrt{2}$, the characteristic impedance of the helium-filled polyester fiber gets undermatched even at low frequencies. The cavity impedance, $\coth(ikt\cos\theta)/\cos\theta$, changes greatly due to the complex refraction angle θ compared with the results for the normal incidence, see Figs. 9(4a) and 9(5a), the magnitude of the cavity impedance decreases significantly, although it is still much larger than that of the characteristic impedance, as shown in Figs. 9(4b) and 9(5b). The final surface impedances shown in Figs. 9(6b) and 9(7b) represent a compromise between the two competing factors, Z_c and $\coth(ikt\cos\theta)/\cos\theta$. For HA, since the large magnitude of $\coth(ikt\cos\theta)/\cos\theta$ is compensated by the small characteristic impedance Z_c, almost perfect impedance match is obtained around the frequency $f_d=0.08$. Accordingly, nearly total absorption is observed in Fig. 9(1a) at this frequency. Alternatively, the impedance matching at oblique incidence can be explained partially by the change in wave propagation direction in the helium-filled porous material. Note that the sound speed in helium gas is about three times as large as that of the air. According to the rule of refraction, when sound wave is incident on the helium-filled absorber at an oblique direction, the penetrated wave is bent toward the air-absorber interface. This results in a longer path of sound propagation and hence more energy dissipation than in the case of air-filled absorber in which the wave is bent toward the normal direction.

As the frequency further increases, the effect of the cavity impedance $\coth(ikt\cos\theta)/\cos\theta$ is reduced and the fact that the characteristic impedance of helium is below that of air takes over. The mismatch of impedance at the air-absorber interface emerges for HA, which leads to a reduction in absorption. This explains the appearance of the peaks in Figs. 8(d) and 9(1b) in the absorption curves for HA.

C. Effect of the protective membrane and duct lining

In practice, an impervious membrane should be installed to separate the helium gas from the ambient air at the air/helium interface. There are two major concerns regarding the use of the protective membrane. The first concern is the gradual loss of helium gas through membrane permeation and the other is the acoustic effect of the membrane on sound penetration. The two concerns are, in fact, related as a thin membrane is required to minimize the negative acoustic impact of the membrane, but an ultrathin membrane will cause serious helium permeation leading to significant loss of helium content and pressure. The much slower infiltration of air into the absorber is negligible in comparison. The question of engineering concern is how long the helium absorber can sustain its nominal performance before the permeation of helium gets so pronounced that its absorption characteristics approach that of the common air-filled sound absorption material. Suppose an aluminum foil of the thickness 2×10^{-5} m is used. The permeation of helium in the porous material can be estimated as follows. The measured permeability coefficient of helium through the aluminum is about $\sigma=1.4\times10^{-21}$ $\mathrm{m^2/Pa\ s}$ (Gerlach *et al.*, 2001). The actual mass permeation rate is proportional to the difference of helium partial pressures at the two sides of the barrier, i.e., membrane, and is inversely proportional to the barrier thickness. The volume flux per unit membrane surface area has the dimension of speed, m/s, which can be understood as the rate of reduction in the thickness of the helium content if the rest is held at the same pressure. For the standard pressure difference of 10^5 Pa, and a membrane thickness of 2×10^{-5} m, the permeation flux is calculated as

$$\dot{q}=\frac{\sigma\Delta p}{\text{thickness}}=\frac{1.4\times10^{-21}\ \mathrm{m^2\ Pa\ s}\times10^5\ \mathrm{Pa}}{0.02\times10^{-3}\ \mathrm{m}}$$
$$=7\times10^{-12}\ \mathrm{m/s}=2.2\times10^{-4}\ \mathrm{m/year}.$$

If the helium-filled absorption layer has a thickness of 5×10^{-2} m, the rate of 2.2×10^{-4} m/year represents a loss of $2.2/500=0.44\%$ of helium. Since the molecule size of oxygen and many other air components is much bigger than that of helium, their permeation rate into the helium absorption layer is much lower than the helium gas. Based on the above analysis, it is reasonable to expect that the helium-filled absorption layer can work for at least 10 years before noticeable changes in acoustic performance may occur.

Another concern for the protective membrane is related to the structural impedance introduced by the membrane. The main effect of a protective membrane layer is its inertia when it is not stretched (Ingard, 1994, p. 1–6; Mechel, 2002, Chap. H.18, Eq. (5); Attenborough and Vér, 2006, p. 272). This is appreciated by looking at the vibration dynamics of the unstretched membrane. If the membrane is located at $y=0$, and sound is incident from $y<0$ at a certain oblique angle, one has (Allard, 1993; Mechel, 2002)

$$m_s i\omega v=p_{\mathrm{air}}-p_{\mathrm{por}}, \tag{22}$$

where m_s, v, p_{air}, and p_{por} are the mass per unit area of the membrane, vibration velocity of the membrane into the porous material, the sound pressures in the air, and porous material sides of the membrane, respectively. The impedance presented to the incident wave, $p_{\mathrm{air}}/v=p_{\mathrm{por}}/v+m_s i\omega$, is the sum of the membrane inertia contribution plus the impedance of the porous material without protection layer, p_{por}/v, which, for the typical case of a layer of finite thickness of t is $p_{\mathrm{por}}/v=(\rho c/\cos\theta)\coth(ikt\cos\theta)$ (Attenborough and Vér 2006, p. 253), where θ is the angle of the sound wave propagating in the sound absorption material. Note that the refracted angle θ is governed by Snell's law, namely, the wavenumber along the interface in the two sides of the air-absorber interface, which is not changed by the presence of the membrane. For the low frequency range considered in this study, the extra structural impedance $m_s i\omega$ reduces the reactance of the total impedance of the absorber. According to Figs. 9(7a) and 9(7b), such changes would lead to lower resonance frequency or lower frequency where absorption is good.

As a measure to evaluate the membrane effect on the absorption performance of the porous material, the transmission loss (TL) of a porous duct lining with and without a protective membrane is measured and compared. The test rig

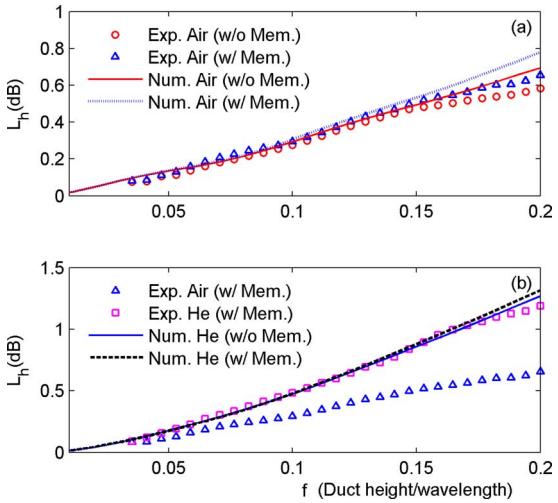

FIG. 11. (Color online) Transmission loss of duct lining. (a) Experimental results for air-filled duct lining covered with membrane (triangle) and without membrane (circle) and theoretical predictions for air-filled duct lining without membrane (solid line) and with membrane (dashed line). (b) Comparison between the experimental results for air-filled (triangle) and helium-filled (square) duct linings covered with membrane, together with comparison between the theoretical predictions for helium-filled duct lining without membrane (solid line) and that with membrane (dashed line).

consists of a rectangular duct with two side-branch cavities flush-mounted on opposite duct walls (Choy and Huang, 2003). The cross section of the duct is 0.2×0.2 m^2, and the two cavities are 5×10^{-2} m in depth and 1 m in length. The polyester fibers with fiber diameter $d=3\times10^{-5}$ m (as investigated in Fig. 5) are filled into the two side-branch cavities to form the so-called duct lining. In order to evaluate the effect of the protective membrane (material: aluminum; thickness: 2×10^{-5} m; aerial density 0.054 kg/m^2), the air-saturated porous material is first tested. Figure 11(a) compares the measured attenuation rate with (open triangles) and without the protective membrane (open circles). The dimensionless frequency f is normalized by the duct height and the speed of sound in air. On the whole, the membrane can improve the low frequency performance, but only slightly. The predicted attenuation rate, L_h, with a finite element model matches the experimental results, especially at low frequencies, where L_h is defined as the reduction in sound dissipation per unit axial distance equal to half of the height of the open part of the lined duct. When helium gas is filled in the side-branch cavities, the protective membrane must be used to separate the helium-filled porous material and the air in the main duct. The open squares in Fig. 11(b) show the measured attenuation rate when helium gas is filled in the side-branch cavities. Again, the measured attenuation rate is in good agreement with the numerical results (dashed line). Compared with the air-filled duct lining (open triangles), the helium-filled duct lining almost doubles the attenuation rate over the calculated frequency range. However, it does not necessarily mean that the helium-filled duct lining outperforms the air-filled duct lining under all design conditions. The particular example shown in Fig. 11 is only to demonstrate the effect of the membrane in a real application. Actually, numerical investigations show that the helium-filled duct lining usually performs better in the low frequency regime, but the air-filled duct linings outperforms in the relatively higher frequency range.

V. CONCLUSIONS

This study is motivated by the desire to extend the effective range of sound absorption by porous material down to lower frequencies, where high acoustic impedance in traditional absorbers prevents sound from ever penetrating into the absorber. The replacement of air by helium gas inside an absorber is shown to have the potential to provide a good low frequency absorber. As a first step in that direction, this study establishes the characteristic of sound propagation in a helium-filled absorption material by experimentation with various fiber configurations. The results are used to predict that a helium-filled absorber of finite thickness would indeed perform well in the low frequency regime. Equivalently, the thickness of such absorber can be reduced for a given absorption coefficient. The conclusion is also confirmed by experimental results in the setting of duct lining. Specific conclusions for this study are as follows.

(1) The speed of sound and complex density, when normalized by those in the pure fluid filling the absorption material, can be expressed as a function of the ratio of fiber dimension, e.g., diameter, to the boundary layer thickness, while the ratio of fiber diameter to the wavelength is less important. The functional relation is the same for absorber filled with air and that filled with helium as far as the porosity and geometrical shape of the fibers are the same. This is experimentally validated.
(2) Helium filled absorption material has a much reduced dimensional characteristic impedance, and so a good impedance match with the impedance of pure air becomes more feasible. This factor allows better sound penetration through the air-absorber interface toward low frequencies.
(3) The performance of an absorber of finite thickness depends also on the sound reflection by the rigid backing and the effective acoustic impedance seen by the incident wave is further increased when the thickness to wavelength ratio is very low. On this account, the performance of a helium-filled absorber is no better, or even worse, than that of ordinary air-filled absorber due to the fact that the wavelength of sound in helium is longer.
(4) When sound is incident at an oblique angle, however, sound is refracted and the comparison between the two absorbers changes in favor of helium, which has a much higher speed of sound. For air-filled absorber, sound penetrating the absorption layer is bent toward the direction perpendicular to the air-absorber interface, reducing the effective distance over which sound can travel in the absorber and get dissipated. For helium-filled absorber, however, the refraction bends the wave toward the air-absorber interface and prolongs the sound travel distance. Such desirable refraction effectively reduces the impedance amplification by the rigid wall backing, and

makes it possible to establish a near-perfect impedance match between the obliquely incident sound in air and the interface impedance of the absorber.

(5) The most important oblique incidence angle is 45° for random incidence. When parameters are chosen suitably, a helium-filled absorber may establish such a near-perfect absorption at certain low frequencies while an air-filled absorber has a monotonous decline of performance with decreasing frequency. The appearance of a spectral peak of absorption coefficient in the spectrum is related to the fact that the characteristic impedance of the helium-filled absorption material can be even lower than the acoustic impedance to be matched for the oblique incidence.

ACKNOWLEDGMENTS

The first author thanks the Hong Kong Polytechnic University for its funding support (Grant No. A-SA43). Likewise, support from a seed fund for applied research at the University of Hong Kong is also acknowledged.

Allard, J. F. (**1993**). *Propagation of Sound in Porous Media Modeling Sound Absorbing Materials* (Elsevier Applied Science, New York).

Allard, J. F., Aknine, A., and Depollier, C. (**1986**). "Acoustical properties of partially reticulated foams with high and medium flow resistance," J. Acoust. Soc. Am. **79**, 1734–1740.

Allard, J. F., and Champoux, Y. (**1992**). "New empirical equations for sound propagation in rigid frame fibrous material," J. Acoust. Soc. Am. **91**, 3346–3353.

Allard, J. F., Depollier, C., Rebillard, P., Lauriks, W., and Corps, A. (**1989**). "Inhomogeneous Biot waves in layered media," J. Appl. Phys. **66**, 2278–2284.

Attenborough, K. (**1982**). "Acoustical characteristics of porous materials," Phys. Rep. **82**, 179–227.

Attenborough, K. (**1983**). "Acoustical characteristics of rigid fibrous absorbents and granular materials," J. Acoust. Soc. Am. **73**, 785–799.

Attenborough, K. (**1987**). "On the acoustic slow wave in air-filled granular materials," J. Acoust. Soc. Am. **81**, 93–102.

Attenborough, K., and Vér, I. L. (**2006**). "Sound-absorbing materials and sound absorbers," in *Noise and Vibration Control Engineering: Principles and Applications*, edited by L. L. Beranek and I. L. Vér (Wiley, New York), Chap. 8.

Blazier, W. E., Jr. (**1997**). "RC Mark II: A refined procedure for rating the noise of heating, ventilating, and air conditioning (HVAC) systems in buildings," Noise Control Eng. J. **45**, 243–250.

Buckingham, E. (**1914**). "On physically similar systems; Illustrations of the use of dimensional equations," Phys. Rev. **4**, 345–376.

Choy, Y. S., and Huang, L. (**2003**). "Drum silencer with shallow cavity filled with helium," J. Acoust. Soc. Am. **114**, 1477–1486.

Delany, M. E., and Bazley, E. N. (**1970**). "Acoustical properties of fibrous materials," Appl. Acoust. **3**, 105–116.

Gerlach, A., Keller, W., Schulz, J., and Schumacher, K. (**2001**). "Gas permeability of adhesives and their application for hermetic packaging of microcomponents," Microsyst. Technol. **7**, 17–22.

Ingard, K. U. (**1994**). *Notes on Sound Absorption Technology* (Noise Control Foundation, New York).

ISO 10534-2, (**1998**). "Determination of sound absorption coefficient and impedance in impedance tubes," International Organization for Standardization.

Johnson, D. L., Koplik, J., and Dashen, R. (**1987**). "Theory of dynamic permeability and tortuosity in fluid-saturated porous media," J. Fluid Mech. **176**, 379–402.

Kirby, R., and Cumming, A. (**1999**). "Prediction of the bulk acoustic properties of fibrous materials at low frequencies," Appl. Acoust. **56**, 101–125.

Lighthill, J. (**1978**). *Waves in Fluids* (Cambridge University Press, Cambridge).

Mechel, F. P. (**1976**). "Model theory for fibrous absorber. Part I: Regular Fibre arrangement; Part II: Model consisting of elementary cells and numerical results," Acustica **36**, 53–89.

Mechel, F. P. (**2002**). *Formulas of Acoustics* (Springer, New York).

Palacio, L., Prádanos, P., Calvo, J. I., and Hernández, A. (**1999**). "Porosity measurements by a gas penetration method and other techniques applied to membrane characterization," Thin Solid Films **348**, 22–29.

Smith, C. D., and Parrot, T. L. (**1983**). "Comparison of three methods for measuring acoustic properties of bulk materials," J. Acoust. Soc. Am. **74**, 1577–1582.

Utsuno, H., Tanaka, T., Fujikawa, T., and Seybert, A. F. (**1989**). "Transfer function method for measuring characteristic impedance and propagation constant of porous materials," J. Acoust. Soc. Am. **86**, 637–643.

Zuckerwar, A. J. (**2002**). *Handbook of the Speed of Sound in Real Gases* (Academic, San Diego, CA).

Zwikker, C. and Kosten, C. W. (**1949**). *Sound Absorbing Materials* (Elsevier, New York).